

Synergistic flame retarded poly(methyl methacrylate) by nano-ZrO₂ and triphenylphosphate

Xinlong Wang · Lianghu Wu · Jin Li

Received: 23 May 2010/Accepted: 13 September 2010/Published online: 7 October 2010
© Akadémiai Kiadó, Budapest, Hungary 2010

Abstract The synergistic flame-retarded systems consisting of nano-ZrO₂ and triphenylphosphate(TPP) for poly(methyl methacrylate)(PMMA) are reported. The synergistic effects were studied by cone calorimeter test, thermal gravimetric analysis (TG), Raman spectra, scanning electron microscopy (SEM), and X-ray photoelectron spectroscopy (XPS). The synergistic effect of nano-ZrO₂ with TPP could be clearly observed by cone calorimeter test. The Raman spectra, SEM, and XPS results provide evidence that nano-ZrO₂ can efficiently promote the formation of charred layers composed of varying amounts of graphite and amorphous carbon. The possible mechanisms for synergy are discussed.

Keywords Poly(methyl methacrylate) · Triphenylphosphate · Synergistic effect · Nano-ZrO₂

Introduction

Poly(methyl methacrylate) (PMMA) is an important thermoplastic material and widely used in numerous industries such as buildings, molding, automobile, and decorative panels. Unfortunately, PMMA is high flammable and thus limited in many applications. The fire resistance of PMMA can be improved by the incorporation of numerous flame retardants, such as inorganic materials, phosphorus-containing and halogen-containing compounds [1–4]. The reduction and substitution of flame retardants containing halogen is progressing in terms of toxicological and

environmental aspects. Organic phosphorus compounds are very effective flame retardants that can be used to reduce the flammability of acrylic polymers. The flame retardancy of them in polymers can act in both the condensed phase and the gas phase. Condensed phase mechanisms increase char formation, which decreases the combustible volatiles and, therefore, the total fuel support of the flame. Furthermore, the char can act as a barrier, decreasing the mass loss rate. Gas phase mechanisms of them reduce the effective heat of combustion by flame inhibition [5]. However, high loadings of organic phosphorus compounds are demanded to provide the required flame retardance (FR). Except for the manufacture cost, high loadings of these additives significantly influence the physical and chemical properties of pristine PMMA. Also, the additives may be leached or otherwise lost from the polymer during service, posing a potential environmental hazard [6]. To address some of the problems associated with the additive route to flame retardance, we have turned our attention to synergy of flame retardancy. In the field of fire retardancy, synergists are often required in order either to sharply improve the performance of materials or to decrease the loading of FR additives while maintaining the performance. Synergistic phenomena can be obtained either by a combination of flame retardancy mechanisms, such as char formation by a phosphorated flame retardant combined with a gas phase action by a halogenated flame retardant, or by a combination of flame retardant agents reinforcing the same mechanism, e.g. nano particles and phosphorated flame retardant agents, both acting in the condensed phase [7, 8].

The triphenylphosphate (TPP) is a kind of widely used commercial flame retardant containing phosphorus which is effective in polymers such as acrylate resins and active in the condensed phase or gas phase. The zirconium

X. Wang (✉) · L. Wu · J. Li
School of Chemical Engineering, Nanjing University of Science and Technology, Nanjing 210094, China
e-mail: wxinlong@sohu.com

compounds are used in fire retardant systems as synergistic agent because they can act as the solid acids that catalyze their dehydrogenation of the polymer. In this article, nano-ZrO₂ is employed to improve flame retardancy of PMMA together with TPP. The thermogravimetry analysis (TG) and cone calorimeter (CONE) are employed to evaluate the synergistic effect and Raman spectra, Scanning Electron Microscopy (SEM) and X-ray photo-electron spectroscopy (XPS) are used to analyse the burnt residues to investigate the synergy mechanism.

Experimental

Materials

Methyl methacrylate (MMA), triphenylphosphate (TPP), *N,N*-dimethylaniline and benzoyl peroxide (BPO) were from Shanghai Lingfeng Chemical Reagent Ltd., China. MMA was redistilled before use. Nano-ZrO₂ was prepared by sol-gel method [9].

Preparation of samples

4 g of PMMA was added to 94 g of MMA, and then oscillated it for 24 h until PMMA was completely dissolved to obtain the MMA dispersion. To a 250 mL beaker, appropriate amount of TPP and nano-ZrO₂, 0.1 g *N,N*-dimethylaniline, and 80 g MMA dispersion were added and stirred for 10 min. Then, 0.3 g BPO was added and stirred for 5 min. The bubbles in the contents of the beaker were removed under vacuum. Then, the mixture in the beaker was poured into the 10 × 10 × 0.3 cm³ glass mold and the mould was heated to 40 °C. After 24 h of polymerization at 40 °C, the plates for testing were obtained. The pure PMMA was prepared under the same experimental conditions. Using MMA dispersion instead of pure MMA for the preparation of nanocomposites could increase the viscosity of the dispersion and reduce the possibility of particle aggregation and phase separation.

Characterization

The cone calorimeter tests were performed according to ISO 5660 standard procedures at a heat flux of 35 kW m⁻² (Stanton Redcroft, UK). The samples used were of dimensions 100 × 100 × 3 mm³. Typical results from cone calorimetry are reproducible to within about ±10%, these uncertainties are based on many runs in which thousands of samples have been combusted. The thermal stability of PMMA and nanocomposites was measured by non-isothermal thermogravimetry method using a DTG-60/60H Simultaneous DTA-TG Apparatus (Shimadzu

Corporation, Japan) from room temperature to 600 °C and the measurements were operated at 20 °C min⁻¹ in nitrogen or air in a flow rate of 20 mL min⁻¹. The laser Raman spectroscopy (LRS) measurements were carried out at room temperature with a laser Raman spectrometer (Invia, Renishaw, UK), with excitation provided in backscattering geometry by a 514.5 nm argon laser line. The surface of solid fire residues was observed by a JEOL-6380LV-type scanning electron microscopy instrument (Electronic Corporation, Japan). XPS analysis was performed with a PHI-5400 spectrometer to study the composition of the residue chars, using Mg K_α excitation radiation (1256.2 eV). The spectrometer was run in fixed analyzer transmission mode at pass energy of 89.45 eV with an X-ray power source of 400 W.

Results and discussion

Structure and characterization of nano-ZrO₂

The shape and size distribution of the nano-ZrO₂ were observed by TEM. Figure 1 showed the image of the prepared nano particles. The diameter of the nano-ZrO₂ was less than 50 nm and the sizes of particles were close to each other, which showed that the distribution was narrow. The typical XRD pattern of prepared nano-ZrO₂ was shown in Fig. 2. The diffraction peaks matched the 001, 111, 200, 202, and 131 crystal planes of nano-ZrO₂ are belong to tetragonal structure.

Cone calorimeter test

Cone calorimeter test is one of the most effective bench scale methods for studying the flammability properties of materials and shows great important significance in the research and development of new flame retardant [10]. The cone calorimeter data obtained are listed in Table 1. Time

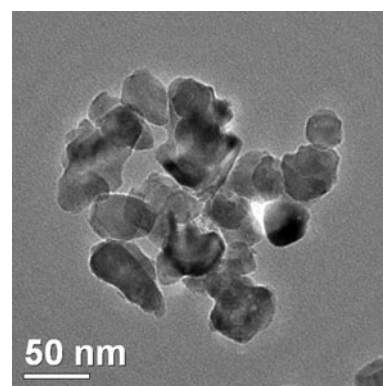


Fig. 1 The TEM photo of nano-ZrO₂

to ignition of PMMA containing TPP was the same as for pure PMMA. In the case of the PMMA nanocomposites containing nano-ZrO₂, the time to ignition is a little increased. The heat release rate curve is given in Fig. 3 as a function of time. From Fig. 3, it can be easily found that the curves have one single peak which is due to the samples' gradual burning. The peak HRR of pure PMMA is 580.38 kW m⁻² and when 20% TPP is added into pure PMMA, the peak HRR has a slight decrease to 556.7 kW m⁻². When nano-ZrO₂ is added into the systems, the PHRRs have obvious reduction as the content of nano-ZrO₂ increases. During combustion, the TPP is known to be active in the condensed phase. The thermal decomposition of TPP leads to the production of phosphoric acid, which condenses readily to produce pyrophosphate structures and liberate water. At high temperature, pyrophosphoric acids are turned into metaphosphoric acid "(O)P(O)(OH)" and their corresponding polymers "(PO₃H)n" [11]. When nano-ZrO₂ was added, ZrO₂ can react with phosphoric acid, pyrophosphoric acids, or polyphosphoric acids to form various kinds of zirconium phosphate. The layers of nano-ZrO₂ and Zr phosphates serve as a barrier to the supply of oxygen and pyrolysis gases. On the other hand, Zr phosphates act as solid acid that can catalyze dehydrogenation of the polymer. Thus,

the pyrolytic products are dehydrogenated and aromatized to form graphitic materials that improve the fire retardancy of PMMA, and which will be proved by Raman spectra. Moreover, the zirconium salts also possesses Lewis acid site Zr⁴⁺ which can capture macroradicals allowing recombination and leading to intermolecular crosslinking [12]. Figure 4 provides the smoke produce rate (SPR) curve of the samples. The SPR decreases obviously while

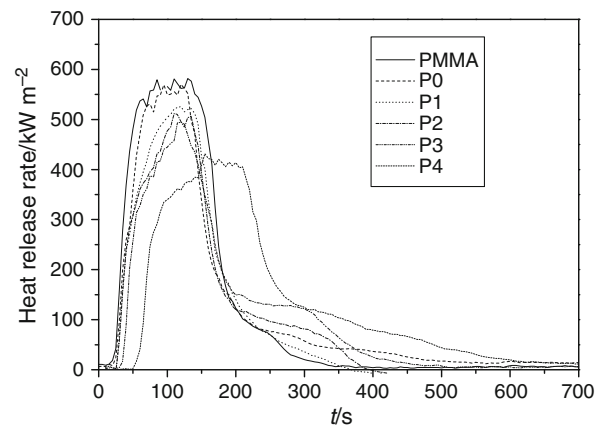


Fig. 3 Heat release rate curves of nanocomposites at a flux of 35 kW m⁻²

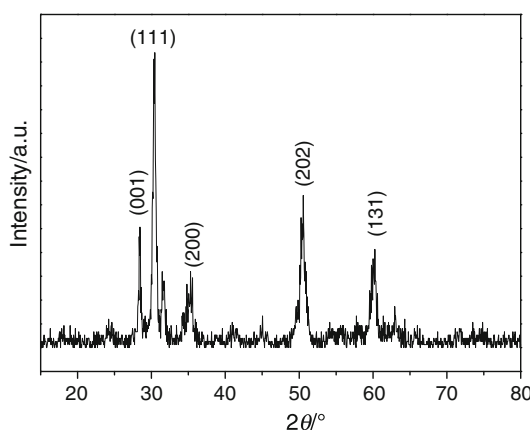


Fig. 2 The XRD pattern of the nano-ZrO₂

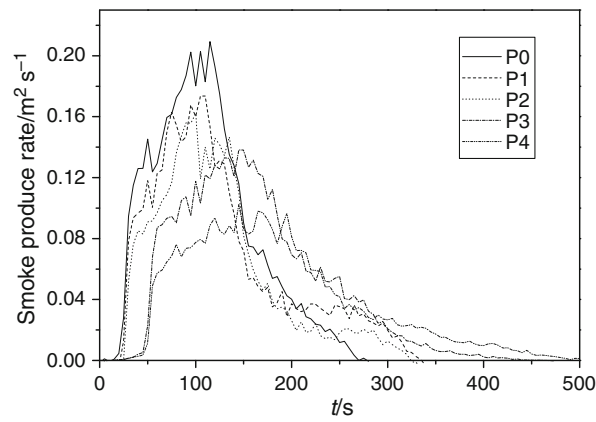


Fig. 4 Smoke produce rate curves of nanocomposites at a flux of 35 kW m⁻²

Table 1 The formulations, cone calorimeter, and Raman spectra data of the samples

Samples	PMMA/wt%	TPP/wt%	ZrO ₂ /wt%	<i>t</i> _{ign} /s	PHRR/kW m ⁻²	THR/MJ m ⁻²	AMLR/gs ⁻¹ m ⁻²	<i>I</i> _D / <i>I</i> _G
PMMA	100	0	0	19	571.74	89.24	17.08	—
P0	80	20	0	19	551.35	88.36	16.51	0.61
P1	80	19.5	0.5	22	525.63	87.89	15.75	0.72
P2	80	19	1	24	512.03	86.04	15.12	0.79
P3	80	17	3	27	475.68	81.26	14.01	0.94
P4	80	15	5	34	428.44	78.89	11.86	0.77

*t*_{ign}, time to ignition, PHRR peak heat release rate, THR total heat release, AMLR average mass loss rate

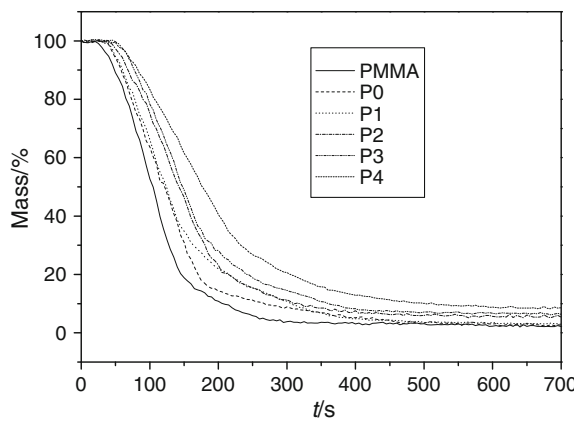


Fig. 5 Mass curves of nanocomposites at a flux of 35 kW m⁻²

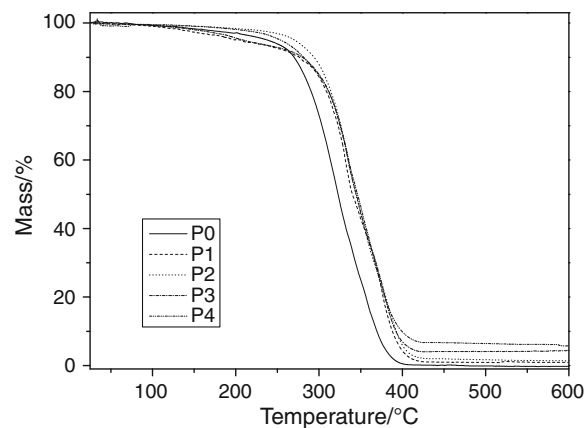


Fig. 7 The TG curves of flame retardant composites under air

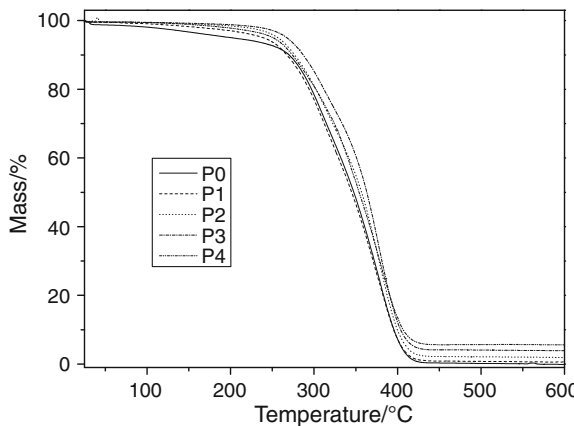


Fig. 6 The TG curves of the flame retardant composites under nitrogen

nano-ZrO₂ is added into the system. The lower smoke production was related to the more dehydrogenated and aromatized aromatic specimen left in the carbonaceous layer, which led to higher char yield. Fig. 5 shows the mass of the char residues and the samples with nano-ZrO₂ have the higher char yields after combustion.

Thermal stability of nanocomposites

The TG curves of the flame-retarded composites under nitrogen and air are shown in Figs. 6, 7, respectively. The data including the temperature at which 10% mass loss occurs (T_{10} , a measure of onset temperature of degradation) and the temperature for 50% degradation (T_{50}) as the mid-point of degradation are used to evaluate the thermal stability. Tests made in the air showed that T_{10} and T_{50} of P0 started at 268.3 and 322.8 °C, while of the nanocomposite with wt 1% of nano-ZrO₂ (P2) at 293.8 and 344.7 °C, respectively. A significant difference in the temperature of degradation initiated in the air, 15.3 and 21.9 °C, indicates the thermal stability improvement. Similar to the results in

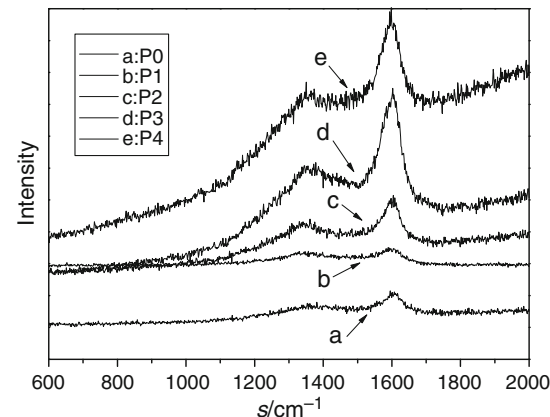


Fig. 8 The Raman spectra of samples after burning

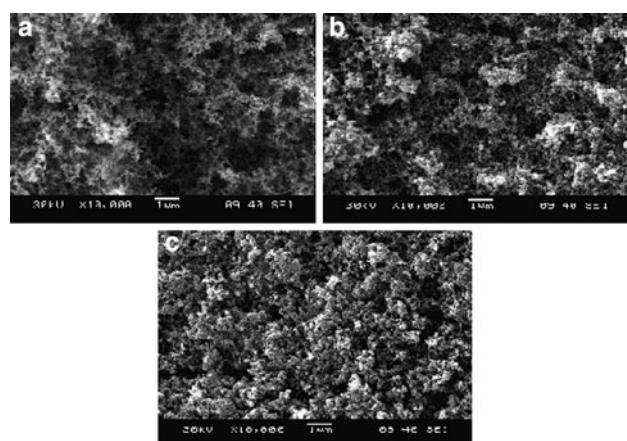


Fig. 9 SEM images of the surface of solid burnt residues **a** P0, **b** P2, **c** P3

air, the composites containing nano-ZrO₂ have a higher decomposition temperature in contrast to that of the PMMA/TPP system under nitrogen. These suggest that nano-ZrO₂ may impede the out-diffusion of the volatile

decomposition products from matrix or in-diffusion of oxygen into matrix [13, 14].

Analysis of the burnt residues

Figure 8 shows the Raman spectra curves of the burnt residues. All curves have two peaks at $1,350\text{ cm}^{-1}$ (peak D) and $1,585\text{ cm}^{-1}$ (peak G) corresponding to the structure of graphite. The ratio of the peak intensity of the D band to

Table 2 Elemental composition and content of the residue chars

Samples	C/wt%	O/wt%	P/wt%	Zr/wt%	P/C	O/C
P0	78.11	19.96	1.93	—	0.025	0.256
P4	59.54	31.40	3.73	4.93	0.063	0.527

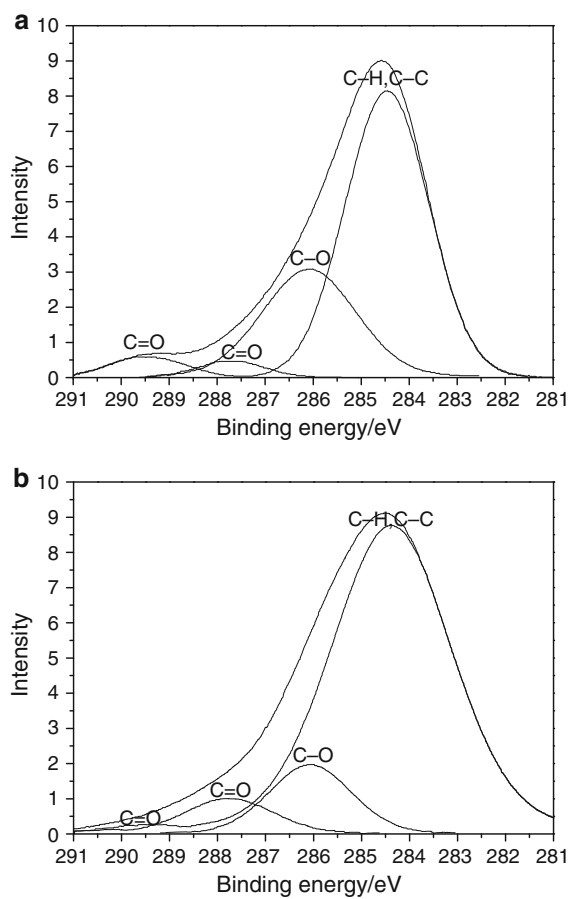


Fig. 10 C_{1s} XPS spectra of residue char **a** P0, **b** P4

the G band and the widths of both peaks are typical parameters to quantify the degree of disorder in carbon materials [15]. In our case, the data for I_D/I_G of all samples are given in Table 1. From Table 1, it can be seen that the values of I_D/I_G for the samples with nano-ZrO₂ are bigger than that of P0. Increasing I_D/I_G indicates a reduction in the total number and/or size of graphitic micro domains, and, therefore, an increase in the number of fourfold coordinated carbon atoms (sp^3/sp^2) in hydrogenated amorphous carbon with increasing hydrogen content. This would cause the higher efficiency of heat shield and improvement of the flame retardance [16].

Figure 9 shows SEM images of the surface of the solid burnt residues. From the Fig. 9, it can be seen that chars turn to be more dense and compact with the addition of nano-ZrO₂. The compact char could prevent the heat transfer and protect material from further burning so as to inhibit the pyrolysis of material and improve its flame retardancy [17].

XPS is surface sensitive in the outermost 2–10 nm of a sample and the elemental and chemical composition of the surface of materials can be obtained [18]. XPS is employed to analyze the elemental composition of residue char. The elemental composition of residue char and the values of P/C and O/C of P0 and P4 are given in Table 2. From the Table 2, it can be seen that phosphorus content and the values of P/C and O/C increased with addition of nano-ZrO₂. This implied that the residue char of the sample with nano-ZrO₂ contained much more phosphorus species and oxidized carbon species.

Figure 10 shows the C_{1s} spectra of the residue char of P0 and P4. There are four peaks located at 289.1, 287.7, 286.1, and 284.6 eV in the C_{1s} spectra curves. The peaks at 289.1 and 287.7 eV are assigned to carbonyl groups. The peaks at 286.1 eV are the contributions of C–O (ether, hydroxyl group, C–O–P in hydrocarbonated phosphate) and the bands around 284.6 eV are assigned to C–H and C–C in aliphatic and aromatic species [19]. The data of the C_{1s} spectra and the values of the ratio of C_{ox} (oxidized carbons) to C_a (aliphatic and aromatic carbons) are listed in Table 3. The values of $\text{C}_{\text{ox}}/\text{C}_a$ of P0 is 0.5542 and when nano-ZrO₂ is added, the value changes into 0.3168 (P4). This indicates that the sample with the nano-ZrO₂ has more aliphatic and aromatic carbons and the nano-ZrO₂ may delay the oxidation of the materials [20].

Table 3 Binding energy (ev) and content (%) of C_{1s} spectra of the residue chars

Samples	Binding energy/ eV	Content/ %	$\text{C}_{\text{ox}}/\text{C}_a$						
P0	289.1	4.22	287.7	3.15	286.1	28.29	284.6	64.34	0.5542
P4	289.1	1.67	287.7	6.38	286.1	11.65	284.5	80.29	0.3168

Conclusions

The nano-ZrO₂ was evaluated in the PMMA/TPP systems as a synergistic agent. The cone calorimeter test results showed when nano-ZrO₂ is added into the system, the PHRRs have obvious reduction as the content of nano-ZrO₂ increases. The TG showed that the addition of nano-ZrO₂ into the nanocomposites can enhance the thermal stability of samples. The results of Raman spectra, SEM, and XPS showed that nano-ZrO₂ influence the carbonaceous char formation and its structure.

Acknowledgements This work was supported by the National Natural Science Foundation of China for the project (No. 20473038) and by the Natural Science Foundation of the Education Committee of Jiangsu province (No. 04KJB150066).

References

1. Wang GA, Wang CC, Chen CY. The flame-retardant material-1. Studies on thermal characteristics and flame retardance behavior of phosphorus-containing copolymer of methyl methacrylate with 2-methacryloxyethyl phenyl phosphate. *Polym Degrad Stab*. 2006;91:2683–90.
2. Price D, Pyrah K, Hull TR, Milnesa GJ, Ebdon JR, Hunt BJ, Joseph P. Flame retardance of poly(methyl methacrylate) modified with phosphorus-containing compounds. *Polym Degrad Stab*. 2002;77:227–33.
3. Lindsay CI, Hill SB, Hearn M, Manton G, Everall N, Bunn A, Heron J, Fletcher I. Mechanisms of action of phosphorus based flame retardants in acrylic polymers. *Polym Int*. 2000;49: 1183–92.
4. Kashiwagi T, Du FM, Douglas JF, Winey KI, Harris RH, Shields JR. Nanoparticle networks reduce the flammability of polymer nanocomposites. *Nat Mater*. 2005;4:928–33.
5. Ulrike B, Bernhard S. Flame retardant mechanisms of red phosphorus and magnesium hydroxide in high impact polystyrene. *Macromol Chem Phys*. 2004;205:2185–96.
6. Giles J. Treaty calls time on long-term pollutants. *Nature*. 2004; 427:768.
7. Serge B, Duquesne S. Fire retardant polymers: recent developments and opportunities. *J Mater Chem*. 2007;17:2283–300.
8. Jiao CM, Chen XL. Synergistic effects of zinc oxide with layered double hydroxides in EVA/LDH composites. *J Therm Anal Calorim*. 2009;98:813–8.
9. Caracoche MC, Rivas PC, Cervera MM, Caruso R, Benavídez E, Oscar DS, Escobar ME. Zirconium oxide structure prepared by the sol–gel route: I, the role of the alcoholic solvent. *J Am Ceram Soc*. 2000;83(2):377–84.
10. Chigwada G, Jash P, Jiang DD, Wilkie CA. Fire retardancy of vinyl ester nanocomposites: synergy with phosphorus-based fire retardants. *Polym Degrad Stab*. 2005;89:85–100.
11. Laoutid F, Bonnaud L, Alexandre M, Lopez-Cuesta J-M, Dubois Ph. New prospects in flame retardant polymer materials: from fundamentals to nanocomposites. *Mater Sci Eng R Rep*. 2009; 63(3):100–25.
12. Yang DD, Hu Y, Song L, Nie SB, He SQ, Cai YB. Catalyzing carbonization function of a-ZrP based intumescent fire retardant polypropylene nanocomposites. *Polym Degrad Stab*. 2008;93: 2014–8.
13. Laachachia A, Cocheza M, Ferriola M, Lopez-Cuestab JM, Leroy E. Influence of TiO₂ and Fe₂O₃ fillers on the thermal properties of poly(methyl methacrylate) (PMMA). *Mater Lett*. 2005;59:36–9.
14. Qin HL, Zhang SM, Zhao CG, Feng M, Yang MS, Shu ZJ, Yang SS. Thermal stability and flammability of polypropylene/mon-tmorillonite composites. *Polym Degrad Stab*. 2004;85:807–13.
15. Hoffmann G, With G, Loos J. Micro-Raman and tip-enhanced Raman spectroscopy of carbon allotropes. *Macromol Symp*. 2008;265:1–11.
16. Ko TH, Kuo WS, Chang YH. Microstructural changes of phenolic resin during pyrolysis. *J App Polym Sci*. 2001;81:1084–9.
17. Demir H, Arkis E, Balkose D. Synergistic effect of natural zeolites on flame retardant additives. *Polym Degrad Stab*. 2005; 89(3):478–83.
18. Gahde J, Loeschke L, Fisher T. XPS investigations on adsorption of polyurethanes and chlorinated poly(vinylchloride) on chromium dioxide. *Acta Polymerica*. 1993;44(3):135–8.
19. Wang ZY, Han EH, Ke W. Effect of acrylic polymer and nanocomposite with nano-SiO₂ on thermal degradation and fire resistance of APP-DPER-MEL coating. *Polym Degrad Stab*. 2006;91:1937–47.
20. Li GX, Yang JF, He TS, Wu YH, Liang GZ. An investigation of the thermal degradation of the intumescent coating containing MoO₃ and Fe₂O₃. *Surf Coat Technol*. 2008;202:3121–8.